Supplementary Information

Human hand-inspired all-hydrogel gripper with a high load capacity formed by the split-brushing adhesion of diverse hydrogels

Hye Been Koo,[a] Eunseok Heo,[a] In Cho,[a] Sun Hong Kim,[b] Jiheong Kang,[a] Jae-Byum Chang*[a]

[a] *Department of Materials Science and Engineering, Korea Advanced Institute of Science and Technology (KAIST), Daejeon 34141, Republic of Korea*

[b] *Department of Electronic Engineering, Hanyang University, Seoul 04763, Republic of Korea*

**Corresponding author: jbchang03@kaist.ac.kr*

Measurement of Breaking Strength. The breaking strengths of the three hydrogels were measured by tensile tests using an universal testing machine (Instron 68SC-1) with a 50 N load cell. Dumbbell-shaped hydrogels with an initial gauge length of 12 mm, width of 2 mm, and thickness of 1 mm were prepared, and their nominal stress-strain curves were recorded at room temperature. Breaking strengths were calculated as the stress at the point of rupture.

Calculation of Work Capacity. The work capacities of these hydrogels were calculated by dividing the work done (J) (force exerted times distance traveled) by the mass of the hydrogel (kg), using the equation below:

$$\text{Work capacity (J kg}^{-1}) = m_w g \Delta h / m_h$$

where m_w is mass of the weight hung under the hydrogel (kg), g is the gravitational acceleration (9.8 m s^{-2}), Δh is the displacement of the weight (m), and m_h is the mass of the hydrogel (kg).

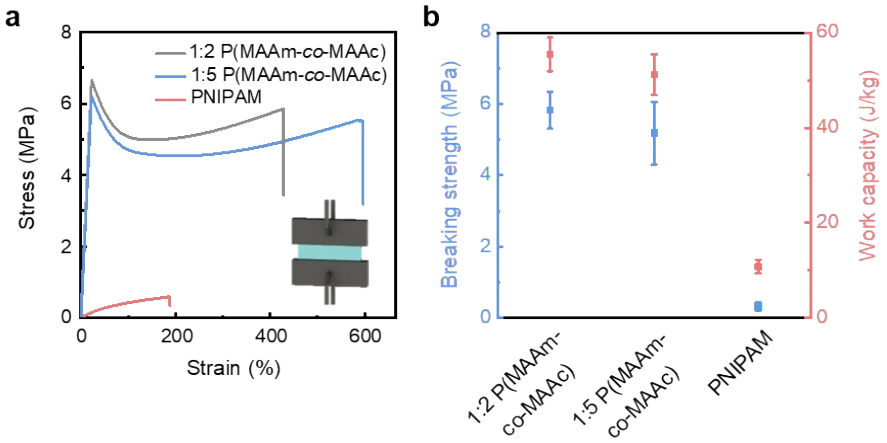

Figure S1. Breaking strengths and work capacities of three temperature-responsive hydrogels: 1:2 P(MAAm-*co*-MAAc), 1:5 P(MAAm-*co*-MAAc), and PNIPAM hydrogels. a) Tensile stress–strain curves of these hydrogels. b) Breaking strengths (blue) measured from the stress–strain curves shown in **a** and work capacities (red) of these hydrogels.

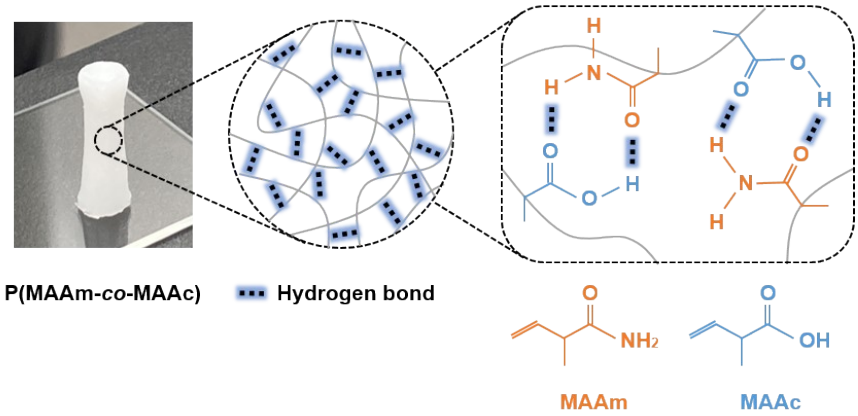

Figure S2. Schematic illustration of P(MAAm-*co*-MAAc) hydrogels based on the formation of robust hydrogen bonds.

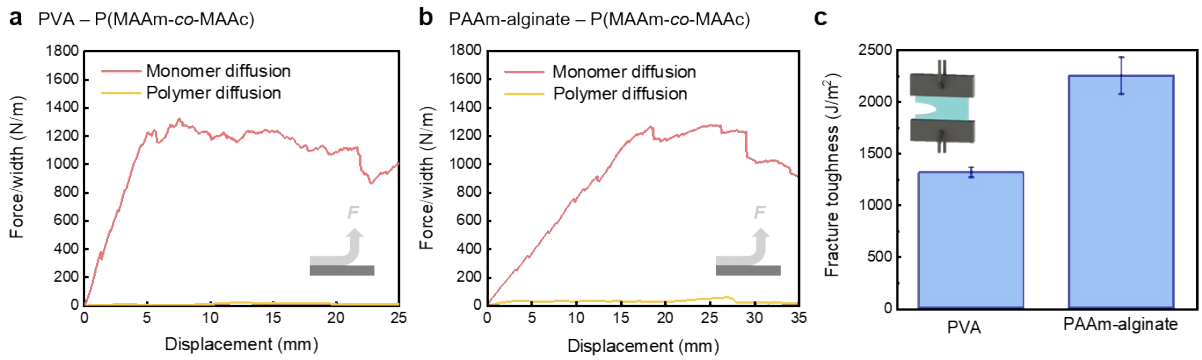

Figure S3. 90°-peeling test and fracture toughness. Representative force/width-displacement curves of the 90°-peeling test via the monomer and polymer diffusion for a) PVA – P(MAAm-*co*-MAAc) and b) PAAm-alginate – P(MAAm-*co*-MAAc) hybrids. c) The measured fracture toughness for PVA and PAAm-alginate hydrogels.

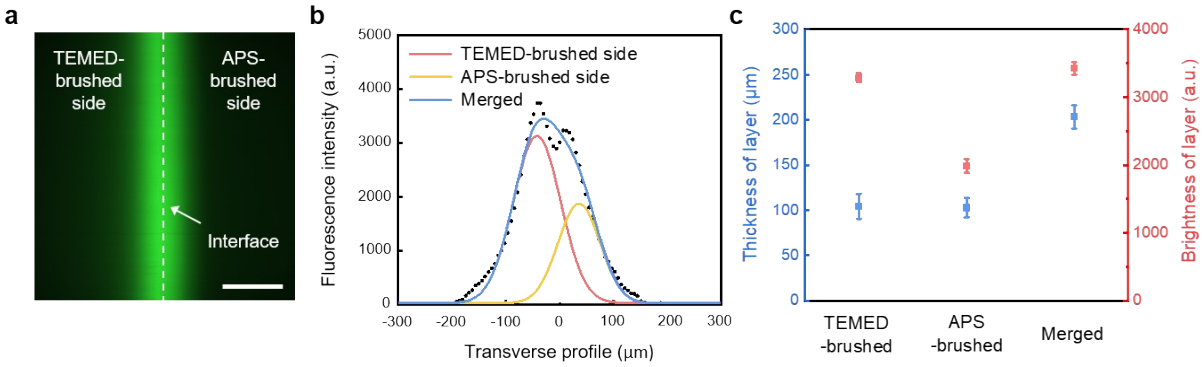

Figure S4. Analysis of fluorescent data for the initiator- and catalyst-brushed sides of two adhered to PAAm hydrogels via split-brushing adhesion. a) Confocal microscopic images of the adhesion interface. The scale bar is 200 μm. b) A representative z-stack profile of the fluorescence intensity. c) The thickness and brightness of the initiator-, catalyst-brushed side, and the entire adhesion interface.

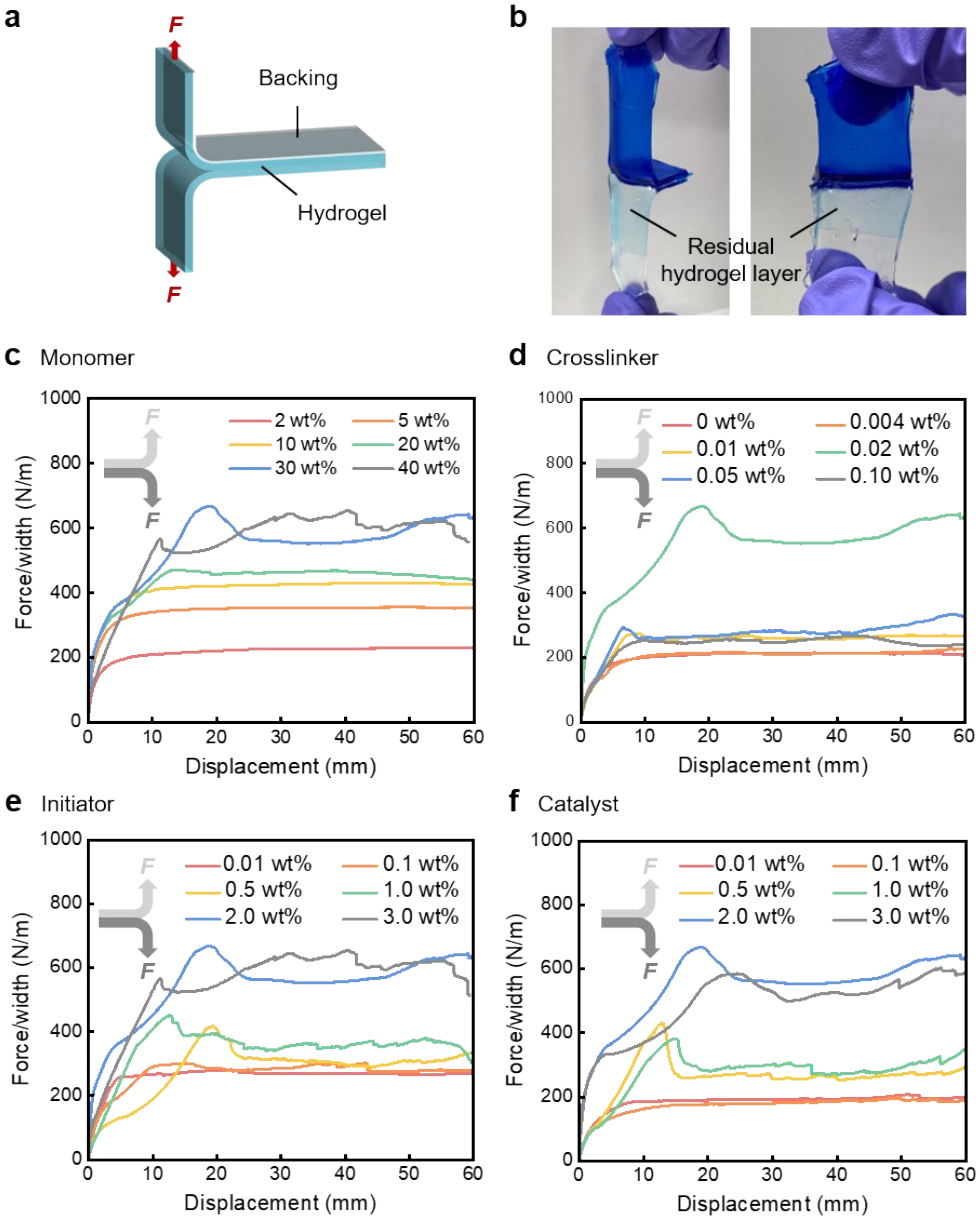

Figure S5. 180°-peeling test for the optimization of split-brushing adhesion. a) Schematic illustration of the 180°-peeling test. b) Photos of the adhesion interface during the 180°-peeling test. Representative force/width-displacement curve of the 180°-peeling test according to the concentrations of the c) monomer, d) crosslinker, e) initiator, and f) catalyst.

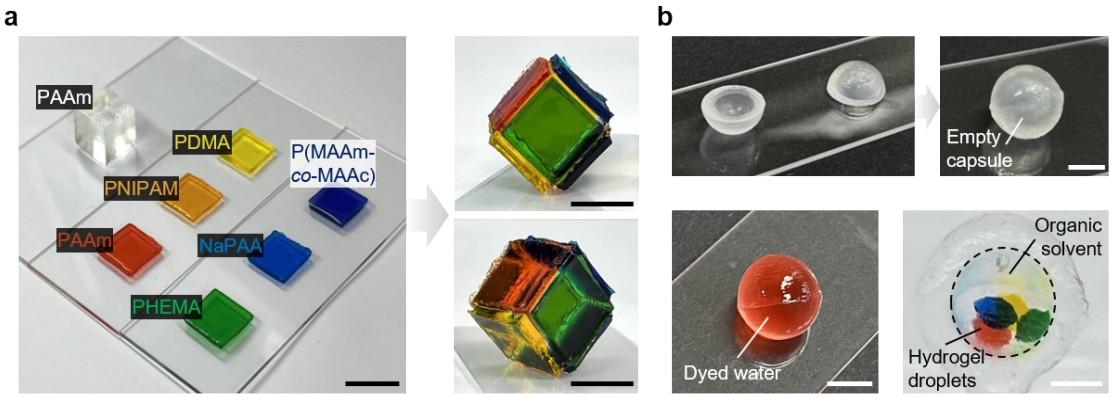

Figure S6. Various 3D heterogeneous structures assembled by the split-brushing adhesion. a) PAAm cube with six types of hydrogel sheets attached to each side. b) Hydrogel capsules containing the solvent and pre-formed hydrogel droplets. All scale bars are 10 mm.

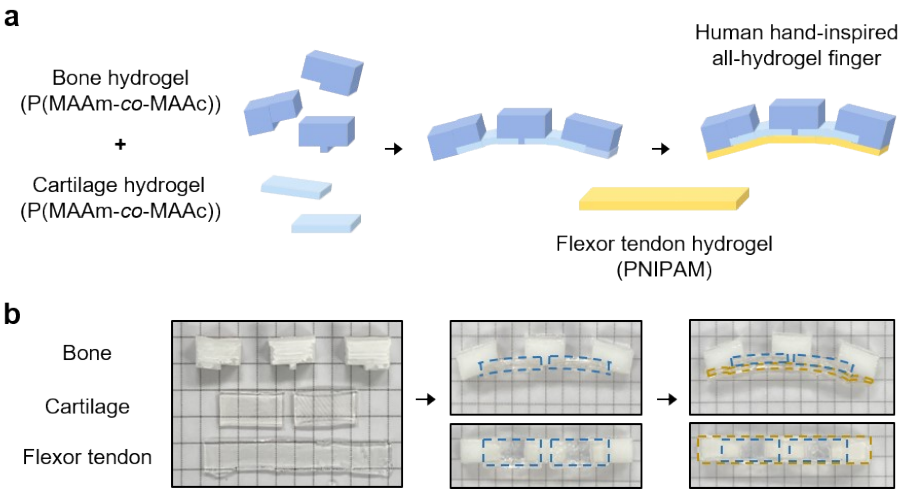

Figure S7. Assembly of the human hand-inspired all-hydrogel finger. (a) Schematic illustration of assembly procedures for the human hand-inspired all-hydrogel finger. Three distinct temperature-responsive hydrogels correspond to each component of the actual human finger, including the bone, cartilage, and flexor tendon. (b) Photos of assembly procedures for the human hand-inspired all-hydrogel finger.

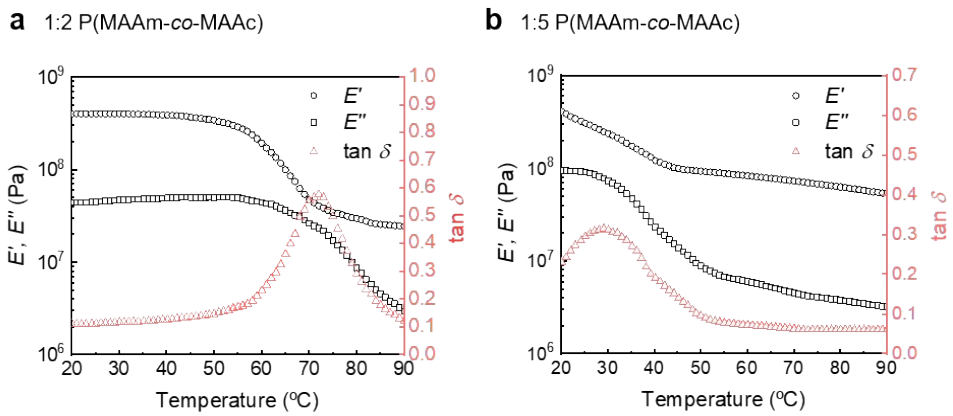

Figure S8. Dynamic mechanical analysis (DMA) spectra and corresponding glass transition temperatures of a) 1:2 and b) 1:5 P(MAAm-*co*-MAAc) hydrogels during the heating process from 20 °C to 90 °C. Sample dimensions: 40 mm × 60 mm × 1 mm. Heating rate: 5 °C/min. DMA test was performed in tensile mode with a frequency of 1 Hz.

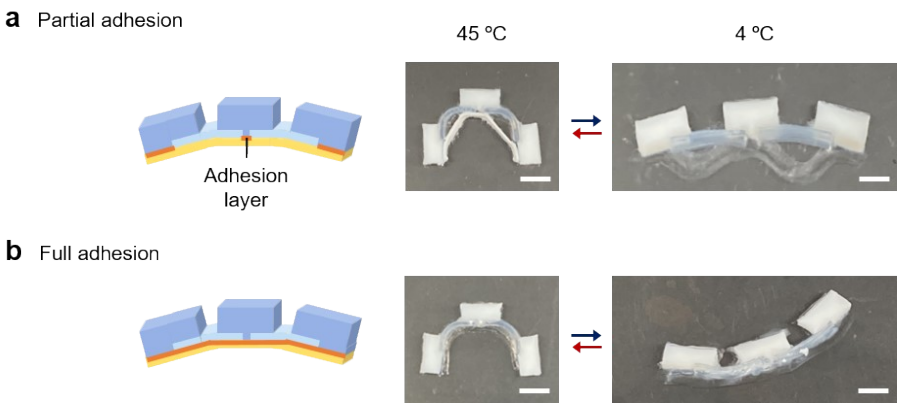

Figure S9. Adhesion between the flexor tendon hydrogel and the bone hydrogel. a) For proper bending of the human hand-inspired all-hydrogel finger, the flexor tendon hydrogel partially adhered to the bone hydrogel. b) As the flexor tendon hydrogel fully adhered to the bone hydrogel, the human hand-inspired all-hydrogel finger was bent in the opposite direction that could not occur in the actual human finger. All scale bars are 10 mm.

Table S1. Performance comparison of previously reported artificial grippers and our gripper.

Water content (wt%)	Young's modulus (MPa)	Number of stimuli	Stimulus	Structure	Maximum bending angle[a]	Actuation speed	Load-to-weight ratio[b]	Ref.
52.9	0.002	1	Pneumatic	Skin-like hydrogel*	< 45º	10 sec	Unknown	1
80	0.0075	1	Pneumatic	Hydrogel coating*	90º	30–240 sec	> 22.2	2
70–98	0.40	1	Temp	Bilayer	60º	150 sec	5	3
86.0–88.9	0.80	1	Salt	Four-layer with hybrid fibers	180º	60 sec	10	4
35.5–45.5	22.9	1	Temp	Bilayer	112.5º	22 sec	17	5
12.7	1	1	Temp	Single layer	90º	30 sec	20	6
48.1	4	1	Electrosm otic	Single layer	80º	10–20 sec	30	7
25–50	< 1	2	Temp pH	Bilayer	135º	35 sec	5	8
< 25	< 1	2	Temp Salt	Bilayer	120º	10 min	23	9
21.6	0.021–0.456	2	Temp Pneumatic	Octopus-like sucker	90º	30 sec	34	10
41.8–94.5	< 1	3	Temp pH salt	A hole in the center	No bending	30 min	~10,000	11
48.5–84.2	**2.3–217.3**	**1**	**Temp**	**Human hand-like**	**101º**	**2–10 min**	**> 47.6**	**This work**

[a] Maximum angle between the two extension lines for the center and the end of grippers

[b] Object mass to gripper mass

[*] Gripper composed of the elastomeric body

References

1 Z. Liu, Y. Wang, Y. Ren, G. Jin, C. Zhang, W. Chen and F. Yan, *Mater. Horizons*, 2020, **7**, 919–927.

2 L. Jing, L. Y. Hsiao, S. Li, H. Yang, P. L. P. Ng, M. Ding, T. Van Truong, S. P. Gao, K. Li, Y. X. Guo, P. Valdivia Y Alvarado and P. Y. Chen, *Mater. Horizons*, 2021, **8**, 2065–2078.

3 M. Hua, D. Wu, S. Wu, Y. Ma, Y. Alsaid and X. He, *ACS Appl. Mater. Interfaces*, 2021, 13, 12689–12697.

4 S. Y. Zheng, Y. Shen, F. Zhu, J. Yin, J. Qian, J. Fu, Z. L. Wu and Q. Zheng, *Adv. Funct. Mater.*, 2018, 28, 1803366.

5 J. Lin, Y. Han, Y. Cui, W. Zhao and C. Chang, *Compos. Part B Eng.*, 2022, 245, 110210.

6 Y. Zhao, C. Y. Lo, L. Ruan, C. H. Pi, C. Kim, Y. Alsaid, I. Frenkel, R. Rico, T. C. Tsao and X. He, *Sci. Robot.*, 2021, 6, 1–12.

7 J. Ko, D. Kim, Y. Song, S. Lee, M. Kwon, S. Han, D. Kang, Y. Kim, J. Huh, J. S. Koh and J. Cho, *ACS Nano*, 2020, 14, 11906–11918.

8 Y. Cheng, K. Ren, D. Yang and J. Wei, *Sensors Actuators, B Chem.*, 2018, 255, 3117–3126.

9 S. Xiao, M. Zhang, X. He, L. Huang, Y. Zhang, B. Ren, M. Zhong, Y. Chang, J. Yang and J. Zheng, *ACS Appl. Mater. Interfaces*, 2018, 10, 21642–21653.

10 S. Zhuo, Z. Zhao, Z. Xie, Y. Hao, Y. Xu, T. Zhao, H. Li, E. M. Knubben, L. Wen, L. Jiang and M. Liu, *Sci. Adv.*, 2020, 6, 1–11.

11 Y. Sun, L. Chen, Y. Jiang, X. Zhang, X. Yao and S. Soh, *Mater. Horizons*, 2019, 6, 160–168.

Video S1. Tough adhesion between various hydrogels via split-brushing adhesion.

Video S2. Single-step cooling pathway for a stiff-bent state.

Video S3. Two-step cooling pathway for a stiff-stretched state.

Video S4. Human-inspired all-hydrogel gripper lifting a heavy object.

Video S5. Fast response of a human hand-inspired all-hydrogel finger with a fast-responsive PNIPAM hydrogel.